



Article

Complexes of Gold(III) with Hydrazones Derived from Pyridoxal: Stability, Structure, and Nature of UV-Vis Spectra

Natalia N. Kuranova, Oleg A. Pimenov, Maksim N. Zavalishin and George A. Gamov *

Department of General Chemical Technology, Ivanovo State University of Chemistry and Technology, Sheremetevskii pr. 7, Ivanovo 153000, Russia; kuranova_nn@isuct.ru (N.N.K.); pimenov@isuct.ru (O.A.P.); zavalishin00@gmail.com (M.N.Z.)

* Correspondence: ggamov@isuct.ru; Tel.: +7(915)821-85-62

Abstract: Pyridoxal and pyridoxal 5'-phosphate are aldehyde forms of B₆ vitamin that can easily be transformed into each other in the living organism. The presence of a phosphate group, however, provides the related compounds (e.g., hydrazones) with better solubility in water. In addition, the phosphate group may sometimes act as a binding center for metal ions. In particular, a phosphate group can be a strong ligand for a gold(III) ion, which is of interest for researchers for the anti-tumor and antimicrobial potential of gold(III). This paper aims to answer whether the phosphate group is involved in the complex formation between gold(III) and hydrazones derived from pyridoxal 5'-phosphate. The answer is negative, since the comparison of the stability constants determined for the gold(III) complexes with pyridoxal- and pyridoxal 5'-phosphate-derived hydrazones showed a negligible difference. In addition, quantum chemical calculations confirmed that the preferential coordination of two series of phosphorylated and non-phosphorylated hydrazones to gold(III) ion is similar. The preferential protonation modes for the gold(III) complexes were also determined using experimental and calculated data.

Keywords: gold(III); hydrazone; pyridoxal; stability constant; speciation; DFT; molecular orbitals; UV-Vis spectra



Citation: Kuranova, N.N.; Pimenov, O.A.; Zavalishin, M.N.; Gamov, G.A. Complexes of Gold(III) with Hydrazones Derived from Pyridoxal: Stability, Structure, and Nature of UV-Vis Spectra. *Int. J. Mol. Sci.* **2024**, *25*, 5046. <https://doi.org/10.3390/ijms25095046>

Academic Editor: Jan Korabecny

Received: 11 April 2024

Revised: 3 May 2024

Accepted: 3 May 2024

Published: 6 May 2024



Copyright: © 2024 by the authors. Licensee MDPI, Basel, Switzerland. This article is an open access article distributed under the terms and conditions of the Creative Commons Attribution (CC BY) license (<https://creativecommons.org/licenses/by/4.0/>).

1. Introduction

Pyridoxal, pyridoxamine, pyridoxine, and their 5'-phosphates (Figure 1) are mutually interconvertible in the living organism and united under the code name B₆ vitamin [1]. These compounds are coenzymes in several dozens of the classified biochemical activities and regulate important processes such as decarboxylation, deamination, and transamination [2]. Both aldehyde forms of B₆ vitamins, pyridoxal (PL), and pyridoxal 5'-phosphate (PLP), can form various Schiff bases and hydrazones that can manifest their own biological activity. In particular, the hydrazone formed by PL and isoniazid, a well-known anti-tubercular agent, (PIH) has long been the subject of extensive research as a potent drug whose biological activity follows from iron-chelating properties [3–7]. The anti-proliferative [8] and thalassemia treatment [9] effects were identified as being among the most promising actions of PIH. In addition, a ferric complex of PIH can provide reticulocytes with iron(III) for heme biosynthesis [10,11]. Anti-oxidative action of PL-derived hydrazones was also reported [12–16]. This could be due to the binding of bivalent metal ions into stable complexes, thus preventing their participation in Fenton-like reactions that lead to the generation of reactive oxygen species. However, ferric complexes of PL-derived hydrazones may have cytotoxic effects because of the induction of oxidative stress [17,18]. In general, hydrazones are versatile compounds gaining attention not only because of their biological activity, but also for their catalytic and fluorescent properties, which can be used for metal recognition and glass and phosphor production [19–21].

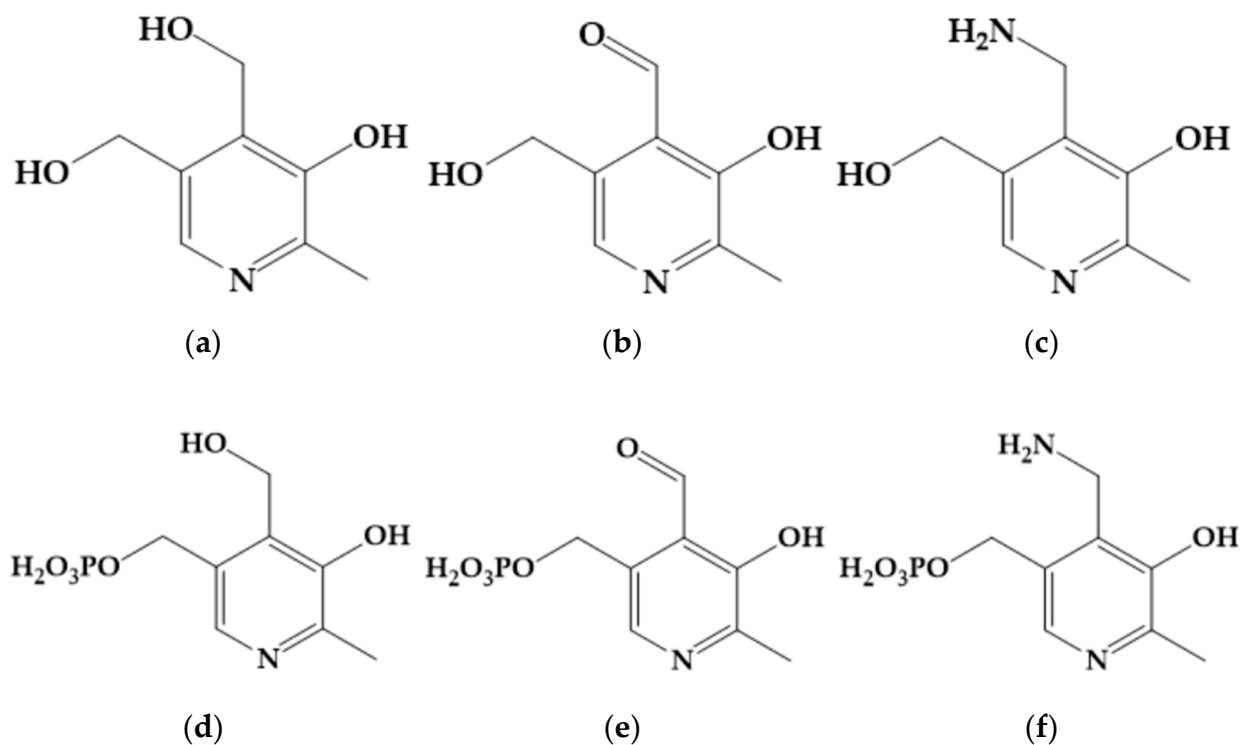


Figure 1. Pyridoxine (a), pyridoxal (b), pyridoxamine (c), pyridoxine 5'-phosphate (d), pyridoxal 5'-phosphate (e), and pyridoxamine 5'-phosphate (f).

PLP-derived hydrazones have received less attention with regard to their biological activity than PL hydrazones. However, the biochemical properties of the phosphorylated hydrazones should be similar to those of PL derivatives. The phosphate group located in the periphery of the molecule does not significantly influence the chelating properties (it is noteworthy that, in general, the peripheral substituents of the hydrazones can be changed significantly without the loss of the most important properties; see, e.g., papers [22–26]). The hydrazone formed by PLP and isoniazid can also show anti-oxidant properties, because it inhibits the copper(II)-mediated oxidation of ascorbic acid due to the ability of Cu^{2+} [27] binding. Comparisons of the stability constants of the complexes formed by Ni^{2+} , Zn^{2+} ions, and PL- and PLP-derived hydrazones [28,29] show that introducing the phosphate group leads to negligible changes in the value of the decimal logarithm of the stability constant ($\log \beta$). In living organisms, hydrazones of pyridoxal 5'-phosphate can form PL-derived compounds as a result of enzymatic dephosphorylation [30]. This process may alter the solubility of hydrazones and their metal complexes, as the phosphate group bearing two protons that can dissociate easily is eliminated from the molecule.

Being low-toxic and membranotropic [31–33], PL-derived hydrazones seem suitable for use in the preparation of metal complexes with biological activity, such as Pt^{2+} or Au^{3+} complexes, as they would help metal ions in permeating the cell membrane. Gold(III) complexes are of special interest, as they are isostructural and isoelectronic to cisplatin, a well-known anti-tumor drug. Hydrazones such as the N,O-donor ligands are a good choice for gold(III), in particular as Au^{3+} 's Lewis acidity corresponds well to the nitrogen and oxygen's Lewis basicity [34]. Different complexes of gold(III) have shown potential anti-tumor [35,36] and antibacterial [37] effects. However, unlike gold(I) compounds that have long been used for arthritis therapy [38], gold(III) compounds are not yet among the approved pharmaceuticals.

Our previous papers [39,40] were devoted to the study of the stability and structure of several gold(III) complexes with hydrazones derived from pyridoxal 5'-phosphate. However, some questions remained unanswered.

First, is the phosphate group involved in the complex formation? Can the partial negative charge accumulated on the phosphate group make it attractive for the cations (including gold(III) species) [40]? This possibility cannot be neglected, as both insoluble [41] and soluble [42] complexes of gold(III) with inorganic phosphate are known, including a valuable histochemical label, so-called black-gold [43–45].

Second, the calculated UV-Vis spectrum of the single protonated complexes of gold(III) with hydrazones has shown the worst agreement with the experimental spectra [40]. What is the reason behind this discrepancy?

Therefore, the present contribution aims to (1) clarify the possible role of the phosphate group in the complexation of B₆ vitamin-derived hydrazones with gold(III) species. To figure out the phosphate effect, it is convenient to study the complexation of gold(III) with pyridoxal hydrazones that are analogous to the PLP derivatives described earlier [39]. (2) Achieve a better agreement between the calculated and experimental UV-Vis spectra for different protonated complexes. The reconsideration of the protonation order is required to solve the problem. (3) Obtain new data on the stability of the complexes of gold(III) and hydrazones derived from pyridoxal. The final goal is to obtain several hydrazones that can be used for the synthesis of gold(III) complexes with antimicrobial and anti-tumor potential. Despite small difference in structure (in the presence or absence of phosphate groups), either PL- or PLP-derived hydrazones may be more beneficial in the end in terms of their biological effect).

The assumed general structural formula of the gold(III) complex with different hydrazones, with an indication of the hypothesized protonation sites, is given in Figure 2.

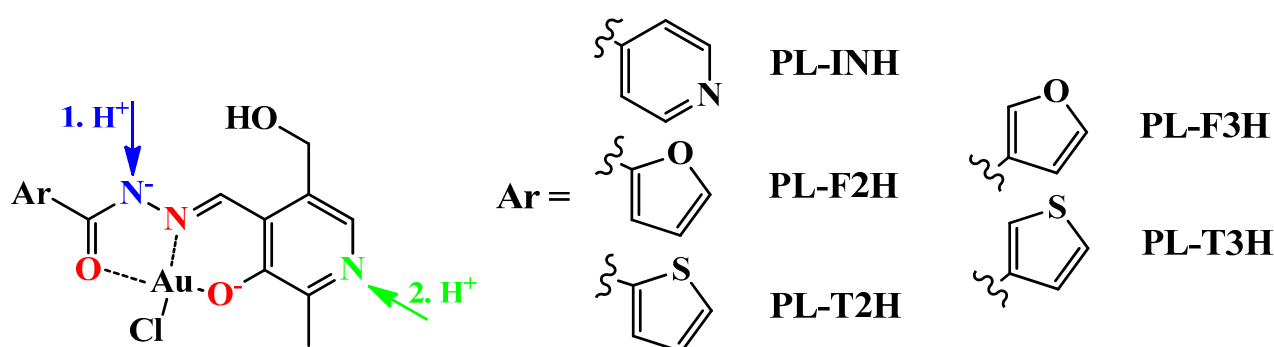


Figure 2. The assumed general structure of the neutral gold(III) complex with the following pyridoxal-derived hydrazones: **PL-INH** (Ar = 4-pyridinyl); **PL-F2H** (Ar = 2-furyl); **PL-F3H** (Ar = 3-furyl); **PL-T2H** (Ar = 2-thienyl); **PL-T3H** (Ar = 3-thienyl). Donor atoms involved in complex formation are marked with red, while acceptors of the first and second protons are marked with blue and green, respectively.

2. Results and Discussion

2.1. Stability of Gold(III) Complexes with Hydrazones

The reasoning described in our previous paper [39] devoted to the gold(III) complexation with PLP-derived hydrazones is also applicable to the complexation with pyridoxal-derived ligands. During the titration, the pH value changed from 3.3 to 9.8 units, which did not cause the precipitate formation.

Examples of spectrophotometric titration are given in Figure 3a,b and Figure S1. These spectral data (similar to those obtained in the previous paper [39]) were used for calculating the stability constants of the gold(III) complexes formed.

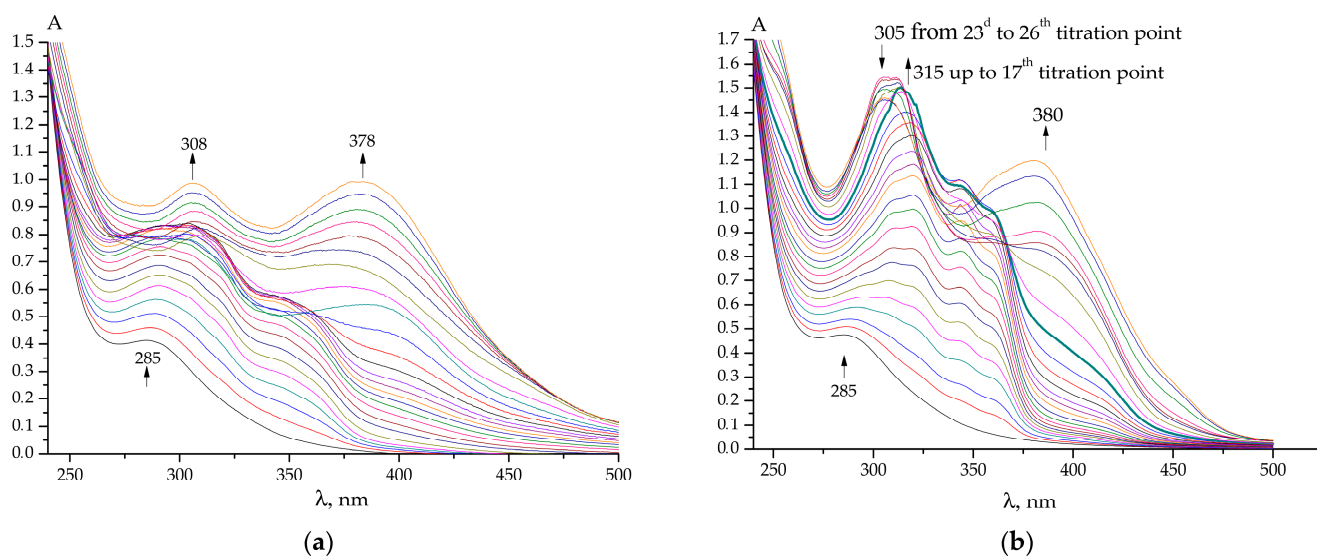
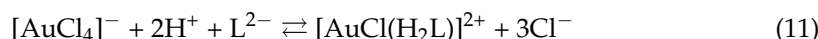
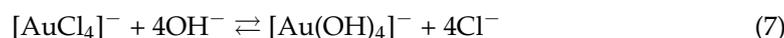
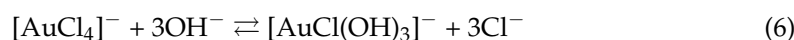
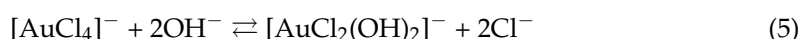
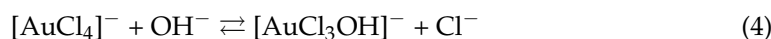


Figure 3. Examples of UV-Vis spectra acquired during the titration of (a) 202.4 μM H[AuCl₄] + 299.4 μM HClO₄ by 1.657 mM PL-INH + 10.34 mM NaOH; and (b) 200.9 μM H[AuCl₄] + 298.9 μM HClO₄ by 1.491 mM PL-T2H + 10.84 mM NaOH in water. Initial volume 2.7 mL, 25 to 30 titration points, titrant volume = 10 μL.

The following processes of the general formula $m\text{H}^+ + n\text{L}^{2-} + p[\text{AuCl}_4]^- + q\text{OH}^- \rightleftharpoons [(\text{AuCl})_p(\text{OH})_q(\text{H}_m\text{L}_n)]^{m+2n+p+q}$ (the overall stability constant for this process is expressed by the following equation: $\beta = [(\text{AuCl})_p(\text{OH})_q(\text{H}_m\text{L}_n)]^{m+2n+p+q} \cdot [\text{H}^+]^{-m} \cdot [\text{L}^{2-}]^{-n} \cdot [[\text{AuCl}_4]^-]^{-p} [\text{OH}^-]^{-q}$) should be set in the stoichiometric scheme for calculations of stability constants using KEV software [46]:



The constants of Processes (1)–(3) are adopted from [47] for PL-INH ($\log \beta_1 = 11.01$; $\log \beta_2 = 19.32$; $\log \beta_3 = 25.38$), PL-F2H ($\log \beta_1 = 11.42$; $\log \beta_2 = 17.94$; $\log \beta_3 = 21.81$), PL-F3H ($\log \beta_1 = 11.97$; $\log \beta_2 = 17.45$; $\log \beta_3 = 22.25$), PL-T2H ($\log \beta_1 = 11.83$; $\log \beta_2 = 17.57$; $\log \beta_3 = 21.57$), and PL-T3H ($\log \beta_1 = 12.0$; $\log \beta_2 = 18.25$; $\log \beta_3 = 21.65$). The constants of Processes (4)–(7) are taken from the paper [48] ($\log \beta_{(4)} = 7.87$; $\log \beta_{(5)} = 14.79$; $\log \beta_{(6)} = 20.92$; $\log \beta_{(7)} = 25.98$). The value of $\log \beta_{(8)} = 13.91$ was taken from the report [49]. The values of $\log \beta$ (Equations (9)–(11)) are to be determined.

As in the previous paper [39], the different stoichiometric models were tested to find the most suitable one. They included the formation of a single complex $[\text{AuCl}(\text{H}_m\text{L})]^m$ ($m = 0-2$), two complexes $[\text{AuCl}(\text{H}_m\text{L})]^m$ and $[\text{AuCl}(\text{H}_{m-1}\text{L})]^{m-1}$ ($m = 1, 2$), and three

complexes (Equations (9)–(11)). The latter gives the best fit of calculated absorbance values to the experimental ones. It should be noted that the hydrazone substitutes three of four chloride anions in the coordination sphere; the last chloride likely remains or is substituted by hydroxyl anion at high pH values (this possibility is taken into account in the model's Equations (4)–(7)). The calculated stability constants, as well as the stepwise protonation constants $\log K_{a1}$ and $\log K_{a2}$, of the complexes ($[\text{AuCl}]\text{L} + \text{H}^+ \rightleftharpoons [\text{AuCl}(\text{HL})]^+$ and $[\text{AuCl}(\text{HL})]^+ + \text{H}^+ \rightleftharpoons [\text{AuCl}(\text{H}_2\text{L})]^{2+}$, respectively; $K_{a1} = \frac{[\text{AuCl}(\text{HL})]^+}{[\text{AuCl}]\text{L} \cdot [\text{H}^+]}$, $K_{a2} = \frac{[\text{AuCl}(\text{H}_2\text{L})]^{2+}}{[\text{AuCl}(\text{HL})]^+ \cdot [\text{H}^]}$, and the constants of gold(III) binding by the protonated ligands, $\log K_{f1}$ and $\log K_{f2}$ ($[\text{AuCl}_4]^- + \text{HL}^- \rightleftharpoons [\text{AuCl}(\text{HL})]^+ + 3\text{Cl}^-$ and $[\text{AuCl}_4]^- + \text{H}_2\text{L} \rightleftharpoons [\text{AuCl}(\text{H}_2\text{L})]^{2+} + 3\text{Cl}^-$, respectively; $K_{f1} = \frac{[\text{AuCl}(\text{HL})]^+ \cdot [\text{Cl}^-]^3}{[\text{AuCl}_4]^- \cdot [\text{HL}^-]}$; and $K_{f2} = \frac{[\text{AuCl}(\text{H}_2\text{L})]^{2+} \cdot [\text{Cl}^-]^3}{[\text{AuCl}_4]^- \cdot [\text{H}_2\text{L}]}$) are given in Table 1.

$$\log K_{a1} = \log \beta([\text{AuCl}(\text{HL})]^+) - \log \beta([\text{AuCl}]\text{L}) \quad (12)$$

$$\log K_{a2} = \log \beta([\text{AuCl}(\text{H}_2\text{L})]^{2+}) - \log \beta([\text{AuCl}(\text{HL})]^+) \quad (13)$$

$$\log K_{f1} = \log \beta([\text{AuCl}(\text{HL})]^+) - \log \beta(\text{HL}^-) \quad (14)$$

$$\log K_{f2} = \log \beta([\text{AuCl}(\text{H}_2\text{L})]^{2+}) - \log \beta(\text{H}_2\text{L}) \quad (15)$$

Table 1. Stability constants of gold(III) complexes with hydrazones derived from pyridoxal in aqueous solution at $T = 298.2 \text{ K}$, $I \sim 0$. The data for the complexes formed by PLP-derived hydrazones [39] are given for comparison.

Hydrazone	PL-INH	PL-F2H	PL-F3H	PL-T2H	PL-T3H
$\log \beta([\text{AuCl}]\text{L})^1$	13.3 ± 0.7	12.0 ± 1.2	12.9 ± 0.6	12.3 ± 0.9	12.5 ± 0.8
$\log \beta([\text{AuCl}(\text{HL})]^+)^1$	21.5 ± 0.8	19.3 ± 0.8	20.2 ± 0.4	20.0 ± 0.6	18.8 ± 0.3
$\log \beta([\text{AuCl}(\text{H}_2\text{L})]^{2+})^1$	25.9 ± 1.4	26 ± 2	25.6 ± 0.1	25.5 ± 1.1	24.3 ± 0.3
$\log K_{a1}^2$	8.2 ± 1.1	7.3 ± 1.4	7.3 ± 0.7	7.7 ± 1.1	6.3 ± 0.9
$\log K_{a2}^2$	4.4 ± 1.6	7 ± 2	5.4 ± 0.4	5.5 ± 1.3	5.5 ± 0.4
$\log K_{f1}^3$	10.5 ± 0.7	7.9 ± 0.8	8.2 ± 0.6	8.2 ± 0.6	6.8 ± 1.0
$\log K_{f2}^3$	6.6 ± 1.4	8 ± 2	8.2 ± 0.3	7.9 ± 1.3	6.0 ± 0.8
Hydrazone [39]	PLP-INH	PLP-F2H	PLP-F3H	PLP-T2H	PLP-T3H
$\log \beta([\text{AuCl}]\text{L})^-$	11.2 ± 0.5	12.4 ± 0.9	12.0 ± 0.5	13.1 ± 0.8	12.5 ± 1.0
$\log \beta([\text{AuCl}(\text{HL})])$	17.8 ± 0.8	18.5 ± 0.6	18.6 ± 0.6	20.3 ± 0.6	18.4 ± 0.3
$\log \beta([\text{AuCl}(\text{H}_2\text{L})]^+)$	23.7 ± 0.9	24.1 ± 0.7	24.7 ± 0.7	26.0 ± 0.5	24.2 ± 0.2
$\log K_{a1}$	6.6 ± 0.9	6.1 ± 1.1	6.6 ± 0.8	7.2 ± 1.0	5.9 ± 1.0
$\log K_{a2}$	5.9 ± 1.2	5.6 ± 0.9	6.1 ± 0.9	5.7 ± 0.8	5.8 ± 0.4
$\log K_{f1}$	6.4 ± 0.9	7.1 ± 0.6	7.2 ± 0.6	8.8 ± 0.6	6.9 ± 1.0
$\log K_{f2}$	4.1 ± 0.9	4.4 ± 0.7	5.0 ± 0.8	6.2 ± 0.7	4.9 ± 0.4

¹ The errors are the half-widths of the confidence interval at a confidence probability of 0.95 and sample size of 4 to 6 experiments; ² The errors are the square roots taken from the sum of squared errors of $\log \beta([\text{AuCl}(\text{H}_m\text{L})]^m)$ that are used for calculations; ³ The errors are the square roots taken from the sum of squared errors of $\log \beta([\text{AuCl}(\text{H}_m\text{L})]^m)$ and protonation constants of hydrazones that are used for calculations.

The complexes of gold(III) formed by pyridoxal-derived hydrazones are slightly more stable than those formed by PLP-derived hydrazones [39]. This small difference can probably be explained by the absence of an electron-withdrawing phosphate group, which favors the formation of the complex. However, the general similarity between the values of stability constants determined for the phosphorylated and dephosphorylated ligands indicates that the phosphate group does not participate in forming the complex with gold(III).

The UV-Vis spectra of the gold(III) complexes with PL-derived hydrazones that were calculated from the experimental data, together with the stability constants, are also similar to those reported for the complexes formed by PLP-derived hydrazones. They are also similar to the spectra of the protonated species (Figures 4a,b and S2).

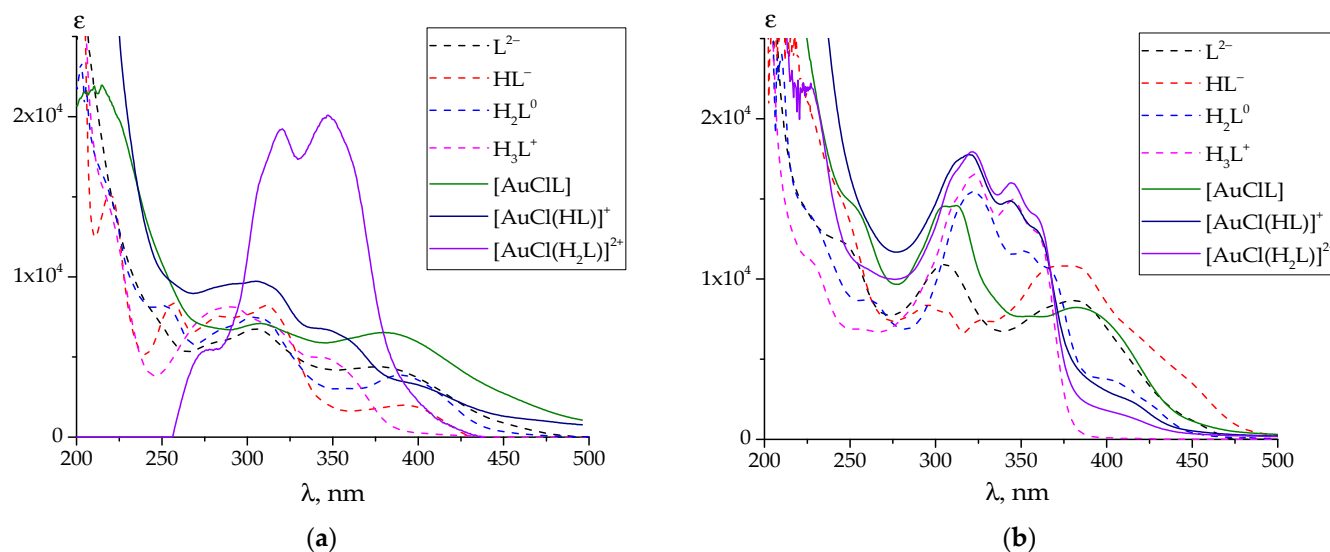


Figure 4. Calculated UV-Vis spectra of individual protonated and complex species of **PL-INH** (a) and **PL-T2H** (b). The protonated species spectra are adopted from [47].

As in the previous paper [39], the relatively high values of the stability constant errors (Table 1) are because of the difficulties experienced while studying the complexation of hydrazones, as well as the similarity of the spectra of protonated and complex species. They are characteristic for such systems, as was noted by the authors of [50].

The speciation diagrams for all the studied complexes for the case of $C(\text{H}[\text{AuCl}_4]) = C(\text{L}) = 0.0001 \text{ mol L}^{-1}$ are shown in Figure S3. In the physiological pH range (7.0 to 7.4), a mixture of $[\text{AuCl}(\text{HL})]^+$ and $[\text{AuCIL}]$ is the predominant species of gold(III). These results can be further used for evaluating the biological activity of gold(III) complexes with hydrazones derived from pyridoxal or calculating the equilibrium composition of the solution containing gold(III) complexes and biological macromolecules such as DNA and proteins.

The speciation diagrams also show that the hydrolysis of gold(III) species is hindered because of complexation with hydrazones.

In the next section, we will discuss the reasons why the UV-Vis spectra of complex gold(III) species look the way they look.

2.2. Geometry of Gold(III) Complexes

To interpret the UV-Vis spectra, DFT calculations of possible molecular models were performed. First, the initial geometry of the gold(III) complexes with **PL**-derived hydrazones was suggested to be analogous with the pyridoxal 5'-phosphate derivatives [40], where the phosphate group is replaced by hydroxyl. The subsequent optimization of the geometrical parameters and the calculation of the harmonic vibration frequencies of gold(III) complexes were carried out for the neutral $[\text{AuCIL}]$ molecule, monoprotinated $[\text{AuCl}(\text{HL})]^+$, and bis-protonated $[\text{AuCl}(\text{H}_2\text{L})]^{2+}$ ions. An interesting observation can be made about the first protonation step: a proton can join two different groups, *viz.*, hydrazide nitrogen and heterocyclic nitrogen belonging to the pyridoxal moiety. Therefore, two possible configurations of monoprotinated species should be considered. The first one, $[\text{AuCl}(\text{HL})]^+$ 1, is a complex where a proton is added to the heterocyclic nitrogen of the pyridoxal residue, while the second one, $[\text{AuCl}(\text{HL})]^+$ 2, is a species where a proton is bound with hydrazide nitrogen. As an example, the considered molecular models of the complex with a **PL-F3H** hydrazone in different protonated states are given in Figure 5.

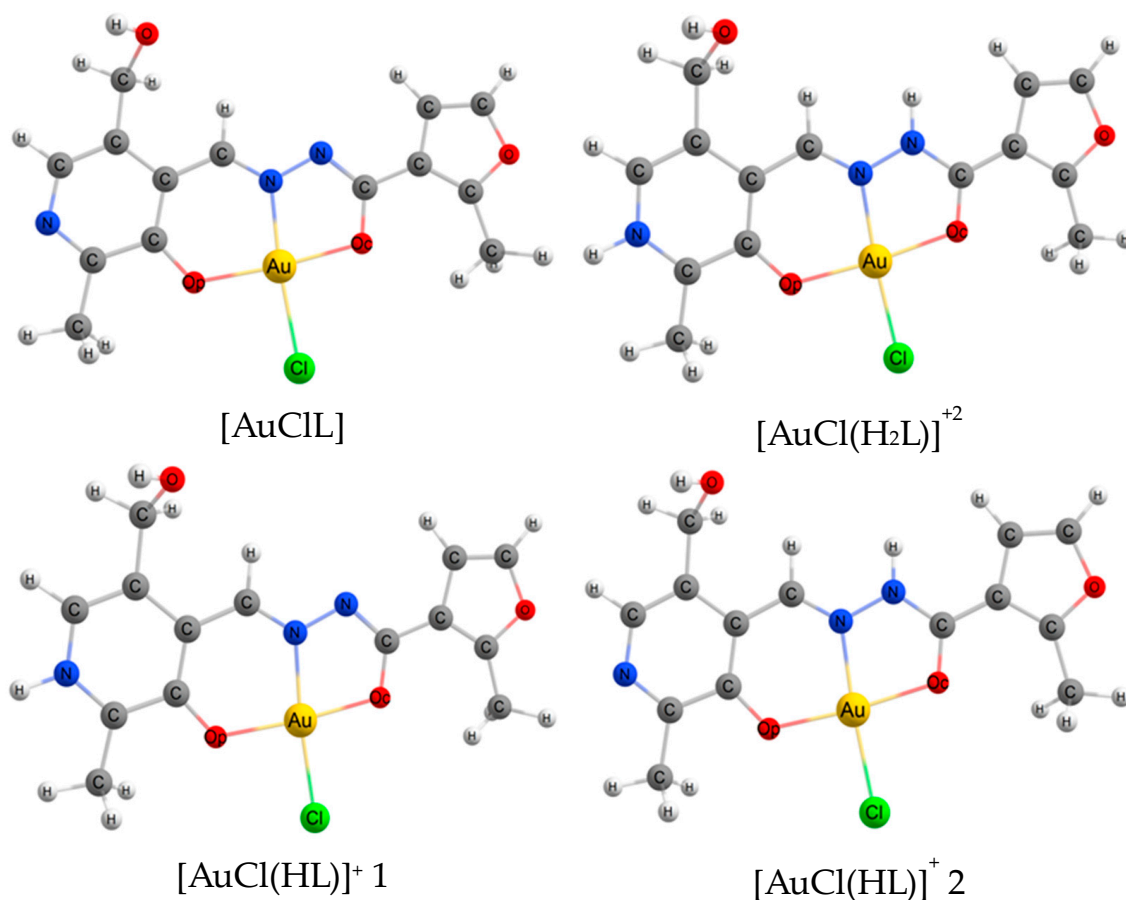


Figure 5. The C_1 symmetry molecular models of neutral ($[\text{AuCl(L)}]$), mono-protonated ($[\text{AuCl(HL)}]^+$ 1, and $[\text{AuCl(HL)}]^{+2}$) and bis-protonated ($[\text{AuCl(H}_2\text{L)}]^{+2}$) forms of complexes formed with **PL-F3H** hydrazone. O_p stands for oxygen of phenyl group in site 3 of pyridoxal moiety; O_c stands for carbonyl oxygen.

There are no imaginary frequencies for all considered molecular models, which means that all of them are minima on the potential energy surfaces (PESs). To test the chemical validity of the proposed gold(III) hydrazone complexes, the theoretical UV–Vis absorption spectra were calculated using TD DFT. The Cartesian coordinates of the C_1 symmetry models of gold(III) complexes with **PL**-derived hydrazones, calculated IR intensities, and energies of vertical electronic transitions and oscillator strengths are presented in the Supplementary Materials Tables S1–S15.

It is noteworthy that we neglected the possibility of phenolic oxygen protonation. A previous study [50] indicated that a completely ionized **PL-INH** hydrazone accepts protons in the following sequence: 1. Hydrazide nitrogen ($\log K = 10.25$) 2. Heterocyclic nitrogen of pyridoxal residue ($\log K = 7.86$) 3. Phenolic oxygen ($\log K = 4.41$) 4. Heterocyclic nitrogen of isoniazid residue ($\log K = 2.95$). In addition, forms of B_6 vitamins tend to form zwitter-ionic species in aqueous solutions with proton transfer from a hydroxyl group to heterocyclic nitrogen [51–55], which likely applies to their hydrazone or Schiff base derivatives.

To simulate the shape of the experimental UV–Vis absorption spectra of the selected molecular models in the range of 200–500 nm, the individual bands were described by Lorentz curves with a half-width of 30 nm. As a result, in Figure 6, the TD DFT simulated UV–Vis absorption spectra are presented both for the complexes of **PL-F3H** and **PLP-F3H** [40] for comparison. For complexes that include other ligands, the observed and simulated UV–Vis absorption spectra are provided in the Figure 3 and Supplementary Materials (Figures S2 and S4).

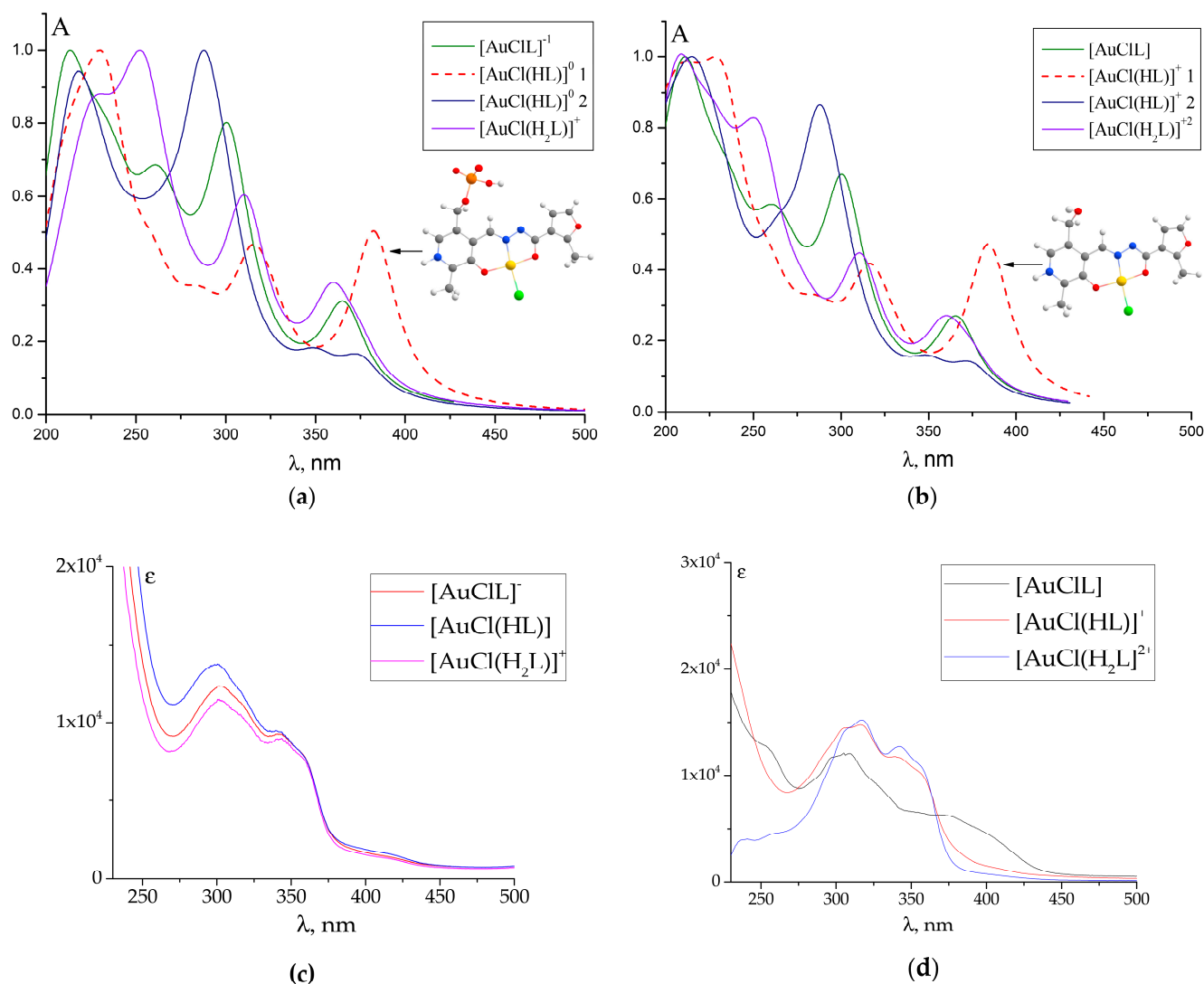


Figure 6. TD DFT (a,b) and experimental (c,d) UV-Vis spectra of different protonated forms of gold(III) complexes with **PLP-F3H** (a,c) and **PL-F3H** (b,d) hydrazones. The red dashed line spectra correspond to single-protonated complexes, where the proton is bound with heterocyclic nitrogen of a **PLP** ($[\text{AuCl}(\text{HL})]^0$ 1) and **PL** ($[\text{AuCl}(\text{HL})]^+$ 1) moiety. The theoretical individual bands were described by Lorentz curves with a half-width of 30 nm.

In the case of the observed UV-Vis spectra of all considered gold(III)-hydrazone complexes (see Figures 4a,b and S2), the sequential protonation $[\text{AuClL}] \rightarrow [\text{AuCl}(\text{HL})]^+ 2 \rightarrow [\text{AuCl}(\text{H}_2\text{L})]^{+2}$ led to a noticeable absorption intensity change rather than a shifting of the spectral bands. For the complex with a **PL-F3H** hydrazone, the TD DFT spectra in the series of $[\text{AuClL}] \rightarrow [\text{AuCl}(\text{HL})]^+ 2 \rightarrow [\text{AuCl}(\text{H}_2\text{L})]^{+2}$ reproduced this tendency better than in the raw $[\text{AuClL}] \rightarrow [\text{AuCl}(\text{HL})]^+ 1 \rightarrow [\text{AuCl}(\text{H}_2\text{L})]^{+2}$. Therefore, we can assume that the calculated UV-Vis spectrum of $[\text{AuCl}(\text{HL})]^+ 2$ agrees better with the experimental one than that of the $[\text{AuCl}(\text{HL})]^+ 1$ complex, which is protonated via heterocyclic nitrogen of **PL** residue.

A similar situation was observed for the gold(III) complexes with **PLP**-derived hydrazones: in the previous paper [40], the worst agreement was found between the calculated and experimental UV-Vis spectra of single-protonated complexes as well. However, they were more difficult cases, as the phosphate group can also accept protons. The most energetically preferable structure was chosen, which was a suboptimal decision, since a significant discrepancy between the calculated and experimental UV-Vis spectra was achieved as a

result. Therefore, in the case of the gold(III) complexes with PL-derived hydrazones, we strongly recommend the $[\text{AuCl}(\text{HL})]^+ 2$ model (which considers a proton to be bound with a hydrazide group) for the interpretation of the chemical properties of a monoprotonated form in an aqueous solution, in spite of the $[\text{AuCl}(\text{HL})]^+ 1$ model being lower in energy.

The geometry of the gold(III) complexes with PL-derived hydrazones is reminiscent of that of the complexes formed by pyridoxal 5'-phosphate derivatives [40], which can be seen from Table 2 data. It presents the bond lengths between the gold(III) ion and donor atoms of the ligands.

Table 2. Equilibrium distances (Å) of AuO_2NCl fragment in gold(III) hydrazone complexes, obtained by DFT/B3LYP calculations.

Distance	PL-F3H	PL-F2H	PL-T3H	PL-T2H	PL-INH
$r(\text{Au}-\text{Cl})$	2.333 *	2.332	2.332	2.332	2.330
	2.302	2.301	2.302	2.302	2.300
	2.293	2.292	2.293	2.292	2.291
$r(\text{Au}-\text{N})$	1.987	1.989	1.988	1.989	1.987
	1.994	1.996	1.994	1.995	1.995
	1.999	2.001	1.999	2.000	2.000
$r(\text{Au}-\text{O}_p)^{**}$	1.980	1.978	1.980	1.978	1.979
	1.969	1.968	1.969	1.968	1.967
	1.971	1.969	1.971	1.969	1.968
$r(\text{Au}-\text{O}_c)^{**}$	2.002	2.005	2.002	2.004	2.004
	2.030	2.032	2.030	2.030	2.038
	2.013	2.015	2.014	2.013	2.021
$r(\text{O}_p \dots \text{O}_c)$	3.979	3.980	3.979	3.978	3.979
	3.996	3.996	3.995	3.994	4.001
	3.980	3.981	3.980	3.979	3.985

* The three horizontal rows for each distance correspond to $[\text{AuClL}]$, $[\text{AuCl}(\text{HL})]^+ 2$, and $[\text{AuCl}(\text{H}_2\text{L})]^{2+}$ forms, respectively. $[\text{AuCl}(\text{HL})]^+ 2$ denotes the monoprotonated complexes, where the proton is bound with hydrazide nitrogen. ** O_p stands for oxygen of a phenyl group in site 3 of pyridoxal moiety; O_c stands for carbonyl oxygen.

The coordination sphere of gold(III) is close to a square planar geometry, as the AuNO_2Cl fragment is close to the D_{4h} ideal reference polygon (see Figure 5). There is a minor difference between the geometries of the complexes formed by PL- and PLP-derived hydrazones, as follows from the DFT calculations. The comparison of the structural parameters of the AuO_2NCl fragment of complexes with PL-F3H and PLP-F3H is presented in Table 3.

The phosphate group, which is remote to the donor atoms of the hydrazones, only slightly influences the complex's structure. However, it is interesting to note that the incorporation of the phosphate group leads to a systematic increase in internuclear distances ($\Delta r > 0$) in the AuO_2NCl fragment (see Table 3), and this tendency is maintained for the remaining complexes as well. The elongation of distances in the coordination cavity of the complex for the phosphorylated ligand is the result of chemical bonds weakening between the gold cation and ligand due to the electron-withdrawing phosphate group effect. Thus, the presented molecular models do not contradict experimental results finding less stability of PLP-derived hydrazones, as mentioned above. The similarity in the structure of PL- and PLP-derived hydrazones, in general, also follows from the similarity of the simulated electronic spectra (see Figure 6).

Table 3. Comparison of equilibrium distances (Å) of AuO₂NCl fragment of gold(III) complexes formed by PL-F3H and PLP-F3H hydrazones, obtained by DFT/B3LYP calculations.

Distance	PL-F3H	PLP-F3H [40]	Δr ***, Å
$r(\text{Au}-\text{Cl})$	2.333 *	2.334 *	0.001
	2.302	2.304	0.002
	2.293	2.294	0.001
$r(\text{Au}-\text{N})$	1.987	1.987	0.000
	1.994	1.995	0.001
	1.999	2.000	0.001
$r(\text{Au}-\text{O}_p)$ **	1.980	1.981	0.001
	1.969	1.970	0.001
	1.971	1.971	0.000
$r(\text{Au}-\text{O}_c)$ **	2.002	2.003	0.001
	2.030	2.032	0.002
	2.013	2.015	0.002
$r(\text{O}_p \dots \text{O}_c)$	3.979	3.980	0.001
	3.996	3.998	0.002
	3.980	3.983	0.003

* The three horizontal rows for each distance correspond to diprotonated, monoprotonated, and *bis*-protonated forms, respectively. The monoprotonated form corresponds to a complex, where the proton is bound with hydrazide nitrogen. ** O_p stands for oxygen of a phenyl group in site 3 of pyridoxal moiety; O_c stands for carbonyl oxygen. *** $\Delta r = r(\text{PL-F3H}) - r(\text{PLP-F3H})$.

The most noticeable changes in the coordination cavity geometry took place during the protonation of the complex. As in the previous paper [40], a significant contraction of Au–Cl (by ~0.04 Å) and elongation of Au–N (by > 0.01 Å) bonds is observed in the series of [AuCIL] → [AuCl(HL)]⁺ 2 → [AuCl(H₂L)]²⁺. Adding a proton in the ligand leads to strong local electron density shift due to electrostatic attraction, which provides the changes in geometry in the coordination cavity and in the ligand.

2.3. The Nature of UV-Vis Absorption Spectra

The results of TD DFT calculations allow for an assignment of the experimental absorption bands. Table 4 summarizes the data on the selected vertical electronic transitions and oscillator strengths corresponding to the absorption band at about 300 and 350 nm for all discussed molecular models of gold(III) with hydrazones. The shapes of the selected molecular orbitals (MOs) with numbering are provided in Table S16.

As in the case of gold(III) complexes with hydrazones derived from pyridoxal 5'-phosphate [40], the positions of the absorption band of the simulated spectra were close to the observed absorption maxima in the vicinity of 300 and 350 nm. In all cases, the absorption bands of the deprotonated species AuL⁰ correspond to $\pi \rightarrow \pi^*$ transitions between ligand MO. The same applies to the complexes with phosphorylated ligands. The first protonation leads to two weak absorption bands arising (~370 and 350 nm) that could be assigned to a $\pi \rightarrow \pi^*$ transition ($S_0 \rightarrow S_2$) and $S_0 \rightarrow S_4$ transition between the chlorine lone pair n_p and LUMO (denoted as σ_{p-d}^*) consisting of gold d-orbital and p-orbitals of N, Cl, and O atoms (see Table S16). A significant contribution into the intensive band in the vicinity of 300 nm is provided by a $\sigma_p \rightarrow \sigma_{p-d}^*$ transition, where σ_p is an MO formed by p-atomic orbitals of pyridoxal moiety. After the second protonation, the single band appears instead of two weak peaks in the 350 nm region, wherein the $\pi \rightarrow \pi^*$ and $\sigma_p \rightarrow \sigma_{p-d}^*$ transitions' contributions are commensurate. The intensive band at 300 nm region mostly appeared due to a $\pi \rightarrow \pi^*$ transition.

Table 4. Selected vertical electronic transitions (UV–Vis absorption spectra), calculated using the TD DFT/CAM-B3LYP method for gold(III) complexes, with hydrazone-derived pyridoxal in aqueous solution.

Hydrazone	Protonated Form	Excited State	λ_{cal} (nm)	Oscillator Strength(<i>f</i>)	Composition *	Character
PL-F3H	[AuCIL]	S ₃	365.97	0.2165	93 ** → 95 (79%), 92 → 95 (11%)	$\pi \rightarrow \pi^*$
		S ₆	301.06	0.5301	92 → 95 (56%), 91 → 95 (30%)	$\pi \rightarrow \pi^*$
	[AuCl(HL)] ⁺ 2	S ₂	374.6	0.0819	93 → 95 (79%), 88 → 94 (12%)	$\pi \rightarrow \pi^*$
		S ₄	349.85	0.0642	88 → 94 (85%), 93 → 95 (15%)	$n_p \rightarrow \sigma_{p-d}^*$
	[AuCl(H ₂ L)] ²⁺	S ₉	287.64	0.6095	92 → 95 (31%), 91 → 94 (27%)	$\pi \rightarrow \pi^*$
		S ₄	359.37	0.1719	90 → 94 (43%), 92 → 95 (25%)	$n_p \rightarrow \sigma_{p-d}^*$
PL-F2H	[AuCIL]	S ₆	311.17	0.342	93 → 95 (46%), 92 → 95 (37%)	$\pi \rightarrow \pi^*$
		S ₃	371.51	0.2062	89 → 91 (61%), 88 → 90 (24%)	$\pi \rightarrow \pi^*$
	[AuCl(HL)] ⁺ 2	S ₆	308.44	0.5742	88 → 91 (81%)	$\pi \rightarrow \pi^*$
		S ₂	377.82	0.117	89 → 91 (77%), 84 → 90 (11%)	$\pi \rightarrow \pi^*$
	[AuCl(H ₂ L)] ²⁺	S ₄	352.67	0.0803	84 → 90 (87%), 89 → 91 (13%)	$n_p \rightarrow \sigma_{p-d}^*$
		S ₉	290.76	0.7339	87 → 90 (39%), 88 → 91 (17%)	$\sigma_p \rightarrow \sigma_{p-d}^*$ $/\pi \rightarrow \pi^*$
PL-T3H	[AuCl(H ₂ L)] ²⁺	S ₄	362.1	0.2309	86 → 90 (42%), 89 → 91 (37%)	$n_p \rightarrow \sigma_{p-d}^*$ $/\pi \rightarrow \pi^*$
		S ₆	305.19	0.7245	88 → 91 (67%), 89 → 92 (14%)	$\pi \rightarrow \pi^*$
	[AuCIL]	S ₃	366.64	0.2199	93 → 95 (92%)	$\pi \rightarrow \pi^*$
		S ₆	300.26	0.5547	92 → 95 (83%)	$\pi \rightarrow \pi^*$
	[AuCl(HL)] ⁺ 2	S ₂	377.02	0.0906	93 → 95 (79%), 87 → 94 (11%)	$\pi \rightarrow \pi^*$
		S ₄	351.09	0.0639	87 → 94 (86%), 93 → 95 (14%)	$n_p \rightarrow \sigma_{p-d}^*$
PL-T2H	[AuCl(H ₂ L)] ²⁺	S ₉	284.03	0.7723	92 → 95 (31%), 91 → 94 (27%)	$\pi \rightarrow \pi^*$
		S ₄	359.82	0.1824	89 → 94 (42%), 93 → 95 (37%)	$n_p \rightarrow \sigma_{p-d}^*$ $/\pi \rightarrow \pi^*$
	[AuCIL]	S ₇	297.69	0.4448	92 → 95 (36%), 91 → 95 (25%)	$\pi \rightarrow \pi^*$
		S ₂	371.3	0.2387	93 → 95 (74%), 92 → 94 (15%)	$\pi \rightarrow \pi^*$
	[AuCl(HL)] ⁺ 2	S ₆	308.01	0.5862	92 → 95 (87%)	$\pi \rightarrow \pi^*$
		S ₂	377.64	0.1172	93 → 95 (76%), 87 → 94 (10%)	$\pi \rightarrow \pi^*$
PL-INH	[AuCl(HL)] ⁺ 2	S ₄	351.66	0.0801	87 → 94 (88%), 93 → 95 (12%)	$n_p \rightarrow \sigma_{p-d}^*$
		S ₉	292.24	0.5032	91 → 94 (40%), 84 → 94 (13%)	$\sigma_p \rightarrow \sigma_{p-d}^*$
	[AuCl(H ₂ L)] ²⁺	S ₄	361.32	0.2194	89 → 94 (48%), 93 → 95 (36%)	$n_p \rightarrow \sigma_{p-d}^*$ $/\pi \rightarrow \pi^*$
		S ₆	307.83	0.6715	92 → 95 (53%), 93 → 96 (19%)	$\pi \rightarrow \pi^*$
	[AuCIL]	S ₂	368.06	0.1511	92 → 94 (79%), 91 → 93 (10%)	$\pi \rightarrow \pi^*$
		S ₆	299.08	0.3955	91 → 94 (85%)	$\pi \rightarrow \pi^*$
[AuCl(HL)] ⁺ 2	S ₂	381.75	0.0681	92 → 94 (72%), 86 → 93 (13%)	$\pi \rightarrow \pi^*$	
	S ₄	357.25	0.0524	86 → 93 (81%), 92 → 94 (16%)	$n_p \rightarrow \sigma_{p-d}^*$	
	S ₁₁	272.04	0.4007	91 → 93 (31%), 90 → 94 (17%)	$\sigma_p \rightarrow \sigma_{p-d}^*$ $/\pi \rightarrow \pi^*$	
[AuCl(H ₂ L)] ²⁺	S ₄	361.84	0.1542	92 → 94 (74%), 88 → 93 (16%)	$\pi \rightarrow \pi^*$	
	S ₁₂	260.17	0.3955	89 → 93 (22%), 86 → 94 (18%)	$\pi \rightarrow \pi^*$	

* The composition includes the first two most significant (%) transitions. The transitions with contributions below 10% are omitted. ** A visualization of molecular orbitals according to the numbers is presented in Supplementary materials (Table S16).

Figure 7 demonstrates frontier MOs of the complex with a PL-F3H hydrazone. The HOMO is of a π -character and localized in the ligand, while the LUMO is σ -antibonding and localized at the center of the coordination cavity, and, as a result, the HOMO→LUMO transition is inactive in gold(III) complexes' absorption spectra. It should be noted that the composition of frontier MOs is the same for the remaining complexes.

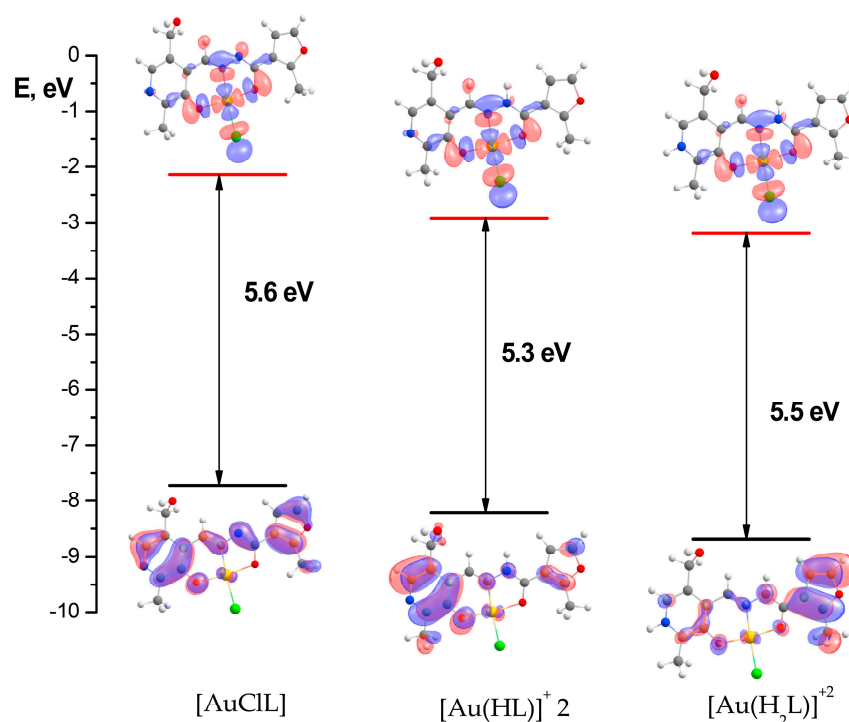


Figure 7. The HOMO–LUMO diagram for deprotonated $[\text{AuClL}]$, monoprotonated $[\text{AuCl}(\text{HL})]^+$, and bis-protonated $[\text{AuCl}(\text{H}_2\text{L})]^{+2}$ forms of the gold(III) complex with a PL-F3H hydrazone.

3. Materials and Methods

3.1. Chemicals

The synthesis and spectral characteristics of PL-F2H and PL-T2H hydrazones are described in a previous paper [29], while the information about PL-INH, PL-F3H, and PL-T3H can be found in paper [47]. $\text{H}[\text{AuCl}_4] \cdot 3.4\text{H}_2\text{O}$ (LenReaktiv, Russia, claimed Au content 49.11%) was used without additional purification. The concentration of perchloric acid used for titration purposes was determined alkalimetrically using the NaOH solution, which was standardized by $\text{Na}_2\text{B}_2\text{O}_7 \cdot 10\text{H}_2\text{O}$. All the solutions for spectral studies were prepared using bidistilled water ($\kappa = 3.6 \mu\text{S cm}^{-1}$, pH = 6.6).

3.2. UV-Vis Titration

UV-Vis spectral titration was performed using a Shimadzu UV1800 double-beam spectrophotometer (Shimadzu, USA, MA) within the spectral range of 200 to 500 nm and absorbance range of 0 to 2. The temperature was maintained at 298.2 ± 0.1 K using an external thermostat. Quartz cells with an optical path of 1.00 cm were used. All experiments were quadruplicated, at least. UV-Vis experiments consisted of the titration of 2.7 mL of the aqueous solution containing 202.4 μM $\text{H}[\text{AuCl}_4]$ and 299.4 μM HClO_4 (total concentration of $\text{H}^+ = 501.7 \mu\text{M}$) in water by an aqueous solution containing hydrazone ($\text{C}(\text{PL-INH}) = 1.657$ mM; $\text{C}(\text{PL-F2H}) = 1.337$ to 1.465 mM; $\text{C}(\text{PL-F3H}) = 1.462$ mM; $\text{C}(\text{PL-T2H}) = 1.491$ mM; $\text{C}(\text{PL-T3H}) = 1.433$ to 1.520 mM) and alkali ($\text{C}(\text{NaOH}) = 9.93$ to 10.84 mM). The volume of titrant added in one injection was 10 μL , and 25 to 30 titration points were acquired in total in each experiment.

Primary UV-Vis spectra were processed using the KEV software, version 0.7 [46] (Accessed (May 4, 2024) to calculate the equilibrium constants of the reaction between gold(III) species and hydrazones. The same software was used for drawing the speciation diagrams.

3.3. Quantum Chemical Calculation Details

The calculations of probable molecular models of gold(III) complexes with the hydrazones derived from pyridoxal were carried out for the singlet electronic state using the Gaussian program package, version 09W [56]. The equilibrium geometrical parameters and normal mode frequencies (Tables S2, S5, S8, S11 and S14) were calculated using the hybrid DFT computational method B3LYP [57]. The energies of vertical electronic transitions and oscillator strengths (UV-Vis spectra) were calculated using the TDDFT [58] method CAM-B3LYP [59]. The two-component relativistic effective core potential (ECP60MDF) [60] was applied for the inner electronic shells of Au ($1s^2 2s^2 2p^6 3s^2 3p^6 3d^{10} 4s^2 4p^6 4d^{10} 4f^{14}$). The valence shells ($5s^2 5p^6 5d^{10} 6s^1$) were described by the (41s37p25d2f1g/5s5p4d2f1g) basis set cc-pVTZ-PP [61]. The H, C, N, O, P, and Cl atomic electronic shells were described by an all-electron cc-pVTZ basis set [62]. To take into account the solvent effect of water, all calculations were performed using the polarizable continuum model (PCM) [63]. The visualization of ball-and-stick models and molecular orbitals was carried out using the CHEMCRAFT program, version 1.8 [64].

4. Conclusions

The stability constants of complexes formed by tetrachloroaurate(III) and five pyridoxal-derived hydrazones in different protonated states were determined using spectrophotometry. Quantum chemical calculations combined with the experimentally determined stability constants, as well as the UV-Vis spectra of protonated species, allowed for the following observations:

- The phosphate group does not participate in the complex formation; however, the electron-withdrawing effect may decrease the complex stability, where the derivatives of pyridoxal 5'-phosphate are involved;
- During the first protonation stage, a proton may bind to different proton-accepting groups. In the case of pyridoxal hydrazones, these groups are the hydrazide nitrogen and heterocyclic nitrogen of pyridoxal residue. The derivatives of PLP have an additional protonation site, the phosphate group. The best agreement between the experimental and calculated UV-Vis spectra was achieved for both PL- and PLP-derived complexes if the first proton was considered to be bound with the nitrogen of the hydrazide group. The total energy value is misleading; based only on this value, the wrong choice of molecular model can be made;
- The spectra of single- and double-protonated complexes of gold(III) are sophisticated. The transition between lone pairs of chlorine and LUMO consisting of both d-orbitals of gold(III) and p-orbitals of donor atoms contribute heavily to the observed peaks. On the contrary, the absorption bands in the spectra of deprotonated complexes are of $\pi \rightarrow \pi^*$ character and involve mostly the ligand MO, with a negligible participation of metal orbitals.

It would be interesting to check in future studies how the change of donor atoms would affect the UV-Vis spectra of the complexes formed by gold(III).

Supplementary Materials: The following supporting information can be downloaded at <https://www.mdpi.com/article/10.3390/ijms25095046/s1>.

Author Contributions: Conceptualization, G.A.G. and O.A.P.; methodology, G.A.G., O.A.P. and N.N.K.; software, G.A.G.; validation, O.A.P., M.N.Z. and N.N.K.; formal analysis, G.A.G.; investigation, O.A.P., M.N.Z. and N.N.K.; resources, G.A.G.; data curation, M.N.Z. and G.A.G.; writing—original draft preparation, M.N.Z. and G.A.G.; writing—review and editing, O.A.P.; visualization, O.A.P.; supervision, G.A.G.; project administration, G.A.G.; funding acquisition, G.A.G. All authors have read and agreed to the published version of the manuscript.

Funding: This research was funded by the Russian Science Foundation, grant number 22-73-10009, <https://rscf.ru/project/22-73-10009/>.

Institutional Review Board Statement: Not applicable.

Informed Consent Statement: Not applicable.

Data Availability Statement: Data are contained within the article or Supplementary Material.

Acknowledgments: We thank G. V. Girichev and A. V. Belyakov for their help in conducting quantum chemical calculations on computing resources of the Department of Physics of ISUCT and Saint Petersburg State Institute of Technology (Technical University). The authors are also grateful to the Center of Collective Use of Ivanovo State University of Chemistry and Technology (supported by the Ministry of Science and Higher Education of Russia, project 075-15-2021-671), because we used its equipment to perform the UV-Vis studies.

Conflicts of Interest: The authors declare no conflicts of interest.

References

1. Bonetti, F.; Brombo, G.; Zuliani, G. The Role of B Group Vitamins and Choline in Cognition and Brain Aging. In *Nutrition and Functional Foods for Healthy Aging*; Elsevier: Amsterdam, The Netherlands, 2017; pp. 139–158. ISBN 978-0-12-805376-8.
2. Liang, J.; Han, Q.; Tan, Y.; Ding, H.; Li, J. Current Advances on Structure-Function Relationships of Pyridoxal 5'-Phosphate-Dependent Enzymes. *Front. Mol. Biosci.* **2019**, *6*, 4. [[CrossRef](#)] [[PubMed](#)]
3. Hoy, T.; Humphrys, J.; Jacobs, A.; Williams, A.; Ponka, P. Effective Iron Chelation Following Oral Administration of an Isoniazid-Pyridoxal Hydrazone. *Br. J. Haematol.* **1979**, *43*, 443–449. [[CrossRef](#)] [[PubMed](#)]
4. Ponka, P.; Borova, J.; Neuwirt, J.; Fuchs, O. Mobilization of Iron from Reticulocytes: Identification of Pyridoxal Isonicotinoyl Hydrazone as a New Iron Chelating Agent. *FEBS Lett.* **1979**, *97*, 317–321. [[CrossRef](#)] [[PubMed](#)]
5. Ponka, P.; Richardson, D.R.; Edward, J.T.; Chubb, F.L. Iron Chelators of the Pyridoxal Isonicotinoyl Hydrazone Class. Relationship of the Lipophilicity of the Apochelator to Its Ability to Mobilise Iron from Reticulocytes in Vitro. *Can. J. Physiol. Pharmacol.* **1994**, *72*, 659–666. [[CrossRef](#)] [[PubMed](#)]
6. Chen, Y.-L.; Kong, X.; Xie, Y.; Hider, R.C. The Interaction of Pyridoxal Isonicotinoyl Hydrazone (PIH) and Salicylaldehyde Isonicotinoyl Hydrazone (SIH) with Iron. *J. Inorg. Biochem.* **2018**, *180*, 194–203. [[CrossRef](#)] [[PubMed](#)]
7. Baker, E.; Richardson, D.; Gross, S.; Ponka, P. Evaluation of the Iron Chelation Potential of Hydrazones of Pyridoxal, Salicylaldehyde and 2-Hydroxy-1-Naphthylaldehyde Using the Hepatocyte in Culture. *Hepatology* **1992**, *15*, 492–501. [[CrossRef](#)] [[PubMed](#)]
8. Richardson, D.; Tran, E.; Ponka, P. The Potential of Iron Chelators of the Pyridoxal Isonicotinoyl Hydrazone Class as Effective Antiproliferative Agents. *Blood* **1995**, *86*, 4295–4306. [[CrossRef](#)] [[PubMed](#)]
9. Szuber, N.; Buss, J.L.; Soe-Lin, S.; Felfly, H.; Trudel, M.; Ponka, P. Alternative Treatment Paradigm for Thalassemia Using Iron Chelators. *Exp. Hematol.* **2008**, *36*, 773–785. [[CrossRef](#)]
10. Ponka, P.; Schulman, H.M.; Wilczynska, A. Ferric Pyridoxal Isonicotinoyl Hydrazone Can Provide Iron for Heme Synthesis in Reticulocytes. *Biochim. Biophys. Acta BBA-Gen. Subj.* **1982**, *718*, 151–156. [[CrossRef](#)]
11. Huang, A.; Ponka, P. A Study of the Mechanism of Action of Pyridoxal Isonicotinoyl Hydrazone at the Cellular Level Using Reticulocytes Loaded with Non-Heme ⁵⁹Fe. *Biochim. Biophys. Acta BBA-Gen. Subj.* **1983**, *757*, 306–315. [[CrossRef](#)]
12. Hermes-Lima, M.; Nagy, E.; Ponka, P.; Schulman, H.M. The Iron Chelator Pyridoxal Isonicotinoyl Hydrazone (PIH) Protects Plasmid pUC-18 DNA against OH-Mediated Strand Breaks. *Free Radic. Biol. Med.* **1998**, *25*, 875–880. [[CrossRef](#)] [[PubMed](#)]
13. Bhattacharya, M.; Ponka, P.; Hardy, P.; Hanna, N.; Varma, D.R.; Lachapelle, P.; Chemtob, S. Prevention of Postasphyxia Electroretinal Dysfunction with a Pyridoxal Hydrazone. *Free Radic. Biol. Med.* **1997**, *22*, 11–16. [[CrossRef](#)] [[PubMed](#)]
14. Hermes-Lima, M. EPR Spin Trapping and 2-Deoxyribose Degradation Studies of the Effect of Pyridoxal Isonicotinoyl Hydrazone (PIH) on ·OH Formation by the Fenton Reaction. *Biochim. Biophys. Acta BBA-Gen. Subj.* **1999**, *1426*, 475–482. [[CrossRef](#)] [[PubMed](#)]
15. Horackova, M. The Antioxidant Effects of a Novel Iron Chelator Salicylaldehyde Isonicotinoyl Hydrazone in the Prevention of H₂O₂ Injury in Adult Cardiomyocytes. *Cardiovasc. Res.* **2000**, *47*, 529–536. [[CrossRef](#)] [[PubMed](#)]
16. Hermes-Lima, M.; Ponka, P.; Schulman, H.M. The Iron Chelator Pyridoxal Isonicotinoyl Hydrazone (PIH) and Its Analogues Prevent Damage to 2-Deoxyribose Mediated by Ferric Iron plus Ascorbate. *Biochim. Biophys. Acta BBA-Gen. Subj.* **2000**, *1523*, 154–160. [[CrossRef](#)] [[PubMed](#)]
17. Buss, J.L.; Neuzil, J.; Ponka, P. The Role of Oxidative Stress in the Toxicity of Pyridoxal Isonicotinoyl Hydrazone (PIH) Analogues. *Biochem. Soc. Trans.* **2002**, *30*, 755–758. [[CrossRef](#)] [[PubMed](#)]
18. Buss, J.L.; Neuzil, J.; Gellert, N.; Weber, C.; Ponka, P. Pyridoxal Isonicotinoyl Hydrazone Analogs Induce Apoptosis in Hematopoietic Cells Due to Their Iron-Chelating Properties. *Biochem. Pharmacol.* **2003**, *65*, 161–172. [[CrossRef](#)] [[PubMed](#)]
19. Laurinaviciute, R.; Ostrauskaite, J.; Skuodis, E.; Grazulevicius, J.V.; Jankauskas, V. Hole-Transporting Phenothiazine-Based Hydrazones with Reactive Vinylbenzyl Groups. *Synth. Met.* **2014**, *192*, 50–55. [[CrossRef](#)]
20. Laurinaviciute, R.; Mimaite, V.; Ostrauskaite, J.; Grazulevicius, J.V.; Jankauskas, V. Hole-Transporting Thiophene-Based Hydrazones with Reactive Vinyl Groups. *Synth. Met.* **2014**, *197*, 1–7. [[CrossRef](#)]
21. Laurinaviciute, R.; Ostrauskaite, J.; Grazulevicius, J.V.; Jankauskas, V. Synthesis, Properties, and Self-Polymerization of Hole-Transporting Carbazole- and Triphenylamine-Based Hydrazone Monomers. *Des. Monomers Polym.* **2014**, *17*, 255–265. [[CrossRef](#)]

22. Astashkin, A.V.; Utterback, R.D.; Sung, Y.-S.; Tomat, E. Iron Complexes of an Antiproliferative Aroyl Hydrazone: Characterization of Three Protonation States by Electron Paramagnetic Resonance Methods. *Inorg. Chem.* **2020**, *59*, 11377–11384. [[CrossRef](#)] [[PubMed](#)]
23. Martins, F.M.; Siqueira, J.D.; Iglesias, B.A.; Chaves, O.A.; Back, D.F. Pyridoxal Water-Soluble Cobalt(II) Helicates: Synthesis, Structural Analysis, and Interactions with Biomacromolecules. *J. Inorg. Biochem.* **2022**, *233*, 111854. [[CrossRef](#)]
24. Qi, J.; Zheng, Y.; Li, B.; Ai, Y.; Chen, M.; Zheng, X. Pyridoxal Hydrochloride Thiosemicarbazones with Copper Ions Inhibit Cell Division via Topo-I and Topo-IIa. *J. Inorg. Biochem.* **2022**, *232*, 111816. [[CrossRef](#)] [[PubMed](#)]
25. Shtyrlin, N.V.; Khaziev, R.M.; Shtyrlin, V.G.; Gilyazetdinov, E.M.; Agafonova, M.N.; Usachev, K.S.; Islamov, D.R.; Klimovitskii, A.E.; Vinogradova, T.I.; Dogonadze, M.Z.; et al. Isonicotinoyl Hydrazones of Pyridoxine Derivatives: Synthesis and Antimycobacterial Activity. *Med. Chem. Res.* **2021**, *30*, 952–963. [[CrossRef](#)]
26. Ahmed, M.A.; Zhernakov, M.A.; Gilyazetdinov, E.M.; Bukharov, M.S.; Islamov, D.R.; Usachev, K.S.; Klimovitskii, A.E.; Serov, N.Y.; Buriilov, V.A.; Shtyrlin, V.G. Complexes of NiII, CoII, ZnII, and CuII with Promising Anti-Tuberculosis Drug: Solid-State Structures and DFT Calculations. *Inorganics* **2023**, *11*, 167. [[CrossRef](#)]
27. Gamov, G.A.; Zavalishin, M.N.; Khokhlova, A.Y.; Gashnikova, A.V.; Sharnin, V.A. Stability of Cu(II) and Zn(II) Complexes with Pyridinecarbohydrazones of Pyridoxal-5-Phosphate in Aqueous Solution. *Russ. J. Gen. Chem.* **2018**, *88*, 1436–1440. [[CrossRef](#)]
28. Gamov, G.A.; Zavalishin, M.N.; Khokhlova, A.Y.; Gashnikova, A.V.; Aleksandriiskii, V.V.; Sharnin, V.A. Complexation between Nickel(II), Cobalt(III) and Hydrazones Derived from Pyridoxal 5'-Phosphate and Hydrazides of 2-,3-,4-Pyridinecarboxylic Acids in Aqueous Solution. *J. Coord. Chem.* **2018**, *71*, 3304–3314. [[CrossRef](#)]
29. Gamov, G.A.; Zavalishin, M.N.; Petrova, M.V.; Khokhlova, A.; Gashnikova, A.V.; Kiselev, A.N.; Sharnin, V.A. Interaction of Pyridoxal-Derived Hydrazones with Anions and Co²⁺, Co³⁺, Ni²⁺, Zn²⁺ Cations. *Phys. Chem. Liq.* **2021**, *59*, 666–678. [[CrossRef](#)]
30. Gamov, G.; Murekhina, A.; Aleksandriiskii, V. Dephosphorylation of Pyridoxal 5'-Phosphate-Derived Schiff Bases in the Presence of Bovine Alkaline Phosphatase. *Int. J. Chem. Kinet.* **2022**, *54*, 58–67. [[CrossRef](#)]
31. Brittenham, G.M. Pyridoxal Isonicotinoyl Hydrazone: Effective Iron Chelation after Oral Administration^a. *Ann. N. Y. Acad. Sci.* **1990**, *612*, 315–326. [[CrossRef](#)]
32. Edward, J.T.; Ponka, P.; Richardson, D.R. Partition Coefficients of the Iron(III) Complexes of Pyridoxal Isonicotinoyl Hydrazone and Its Analogs and the Correlation to Iron Chelation Efficacy. *Biomaterials* **1995**, *8*, 209–217. [[CrossRef](#)]
33. Buss, J.L.; Arduini, E.; Ponka, P. Mobilization of Intracellular Iron by Analogs of Pyridoxal Isonicotinoyl Hydrazone (PIH) Is Determined by the Membrane Permeability of the Iron–Chelator Complexes. *Biochem. Pharmacol.* **2002**, *64*, 1689–1701. [[CrossRef](#)] [[PubMed](#)]
34. Patanjali, P.; Kumar, R.; Sourabh; Kumar, A.; Chaudhary, P.; Singh, R. Reviewing Gold(III) Complexes as Effective Biological Operators. *Main Group Chem.* **2018**, *17*, 35–52. [[CrossRef](#)]
35. Bertrand, B.; Williams, M.R.M.; Bochmann, M. Gold(III) Complexes for Antitumor Applications: An Overview. *Chem.-Eur. J.* **2018**, *24*, 11840–11851. [[CrossRef](#)] [[PubMed](#)]
36. Gurba, A.; Taciak, P.; Sacharczuk, M.; Młynarczuk-Biały, I.; Bujalska-Zadrożny, M.; Fichna, J. Gold (III) Derivatives in Colon Cancer Treatment. *Int. J. Mol. Sci.* **2022**, *23*, 724. [[CrossRef](#)] [[PubMed](#)]
37. Ratia, C.; Sueiro, S.; Soengas, R.G.; Iglesias, M.J.; López-Ortiz, F.; Soto, S.M. Gold(III) Complexes Activity against Multidrug-Resistant Bacteria of Veterinary Significance. *Antibiotics* **2022**, *11*, 1728. [[CrossRef](#)] [[PubMed](#)]
38. Bakhromi, D.; Safarmamadzoda, S.M.; Fritskii, I.O.; Muborakkadamov, D.A. Complex formation of gold (i) with 2-methylimidazole. *ChemChemTech* **2023**, *66*, 27–34. [[CrossRef](#)]
39. Kuranova, N.N.; Yarullin, D.N.; Zavalishin, M.N.; Gamov, G.A. Complexation of Gold(III) with Pyridoxal 5'-Phosphate-Derived Hydrazones in Aqueous Solution. *Molecules* **2022**, *27*, 7346. [[CrossRef](#)] [[PubMed](#)]
40. Pimenov, O.A.; Grazhdan, K.V.; Zavalishin, M.N.; Gamov, G.A. Geometry and UV-Vis Spectra of Au³⁺ Complexes with Hydrazones Derived from Pyridoxal 5'-Phosphate: A DFT Study. *Int. J. Mol. Sci.* **2023**, *24*, 8412. [[CrossRef](#)]
41. Panagiotidis, K.; Glaum, R.; Der Günne, J.S.A.; Hoffbauer, W. Pd₂P₂O₇ AND AuPO₄-NEW ANHYDROUS PHOSPHATES OF NOBLE METALS. *Phosphorus Res. Bull.* **2005**, *19*, 77–82. [[CrossRef](#)]
42. Adam, A.M.A.; Refat, M.S.; Ismail, L.A.; Naglah, A.M.; Al-Omar, M.A.; Al-Wasidi, A.S. Insights into the Complexation of Glucose-6-Phosphate (G6P) with V(III), Ru(III), Au(III), and Se(IV) Ions in Binary Solvent System. *J. Mol. Liq.* **2019**, *296*, 111999. [[CrossRef](#)]
43. Schmued, L.C. Histochemical Labeling Stain for Myelin in Brain Tissue. U.S. Patent No. 6,372,451, 16 April 2002.
44. Schmued, L.; Slikker, W. Black-Gold: A Simple, High-Resolution Histochemical Label for Normal and Pathological Myelin in Brain Tissue Sections. *Brain Res.* **1999**, *837*, 289–297. [[CrossRef](#)] [[PubMed](#)]
45. Schmued, L.; Bowyer, J.; Cozart, M.; Heard, D.; Binienda, Z.; Paule, M. Introducing Black-Gold II, a Highly Soluble Gold Phosphate Complex with Several Unique Advantages for the Histochemical Localization of Myelin. *Brain Res.* **2008**, *1229*, 210–217. [[CrossRef](#)] [[PubMed](#)]
46. Meshkov, A.N.; Gamov, G.A. KEV: A Free Software for Calculating the Equilibrium Composition and Determining the Equilibrium Constants Using UV-Vis and Potentiometric Data. *Talanta* **2019**, *198*, 200–205. [[CrossRef](#)]
47. Kuranova, N.N.; Petrova, D.V.; Zavalishin, M.N.; Kiselev, A.N.; Gamov, G.A. Prediction of Protonation Constants of Hydrazones and Schiff Bases Derived from Pyridoxal 5'-Phosphate, Pyridoxal, 3-Hydroxyisonicotinaldehyde and Salicylic Aldehyde. *J. Mol. Liq.* **2023**, *390*, 123049. [[CrossRef](#)]

48. Mironov, I.V.; Tselodub, L.D. Chlorohydroxide Complexes of Gold(III) in Aqueous Alkali Solutions. *Zhurnal Neorganicheskoi Khimii* **2000**, *45*, 706–711.
49. Bandura, A.V.; Lvov, S.N. The Ionization Constant of Water over Wide Ranges of Temperature and Density. *J. Phys. Chem. Ref. Data* **2006**, *35*, 15–30. [[CrossRef](#)]
50. Wis Vitolo, L.M.; Hefter, G.T.; Clare, B.W.; Webb, J. Iron Chelators of the Pyridoxal Isonicotinoyl Hydrazone Class Part II. Formation Constants with Iron(III) and Iron(II). *Inorganica Chim. Acta* **1990**, *170*, 171–176. [[CrossRef](#)]
51. Sánchez-Ruiz, J.M.; Llor, J.; Cortijo, M. Thermodynamic Constants for Tautomerism and Ionization of Pyridoxine and 3-Hydroxypyridine in Water–Dioxane. *J. Chem. Soc. Perkin Trans.* **1984**, *2*, 2047–2051. [[CrossRef](#)]
52. Llor, J.; Asensio, S.B. Thermodynamics of the Solution Equilibria of 3-Hydroxypyridine and Pyridoxine in Water–Dioxane Mixtures. *J. Solut. Chem.* **1995**, *24*, 1293–1305. [[CrossRef](#)]
53. Llor, J.; Muñoz, L. Tautomeric Equilibrium of Pyridoxine in Water. Thermodynamic Characterization by ^{13}C and ^{15}N Nuclear Magnetic Resonance. *J. Org. Chem.* **2000**, *65*, 2716–2722. [[CrossRef](#)] [[PubMed](#)]
54. Chan-Huot, M.; Niether, C.; Sharif, S.; Tolstoy, P.M.; Toney, M.D.; Limbach, H.-H. NMR Studies of the Protonation States of Pyridoxal-5'-Phosphate in Water. *J. Mol. Struct.* **2010**, *976*, 282–289. [[CrossRef](#)]
55. Limbach, H.-H.; Chan-Huot, M.; Sharif, S.; Tolstoy, P.M.; Shenderovich, I.G.; Denisov, G.S.; Toney, M.D. Critical Hydrogen Bonds and Protonation States of Pyridoxal 5'-Phosphate Revealed by NMR. *Biochim. Biophys. Acta BBA-Proteins Proteom.* **2011**, *1814*, 1426–1437. [[CrossRef](#)] [[PubMed](#)]
56. Frisch, M.J.; Trucks, G.W.; Schlegel, H.B.; Scuseria, G.E.; Robb, M.A.; Cheeseman, J.R.; Scalmani, G.; Barone, V.; Petersson, G.A.; Nakatsuji, H.; et al. *Gaussian 09, Revision A.02*; Gaussian Inc.: Wallingford, CT, USA, 2016.
57. Stephens, P.J.; Devlin, F.J.; Chabalowski, C.F.; Frisch, M.J. Ab Initio Calculation of Vibrational Absorption and Circular Dichroism Spectra Using Density Functional Force Fields. *J. Phys. Chem.* **1994**, *98*, 11623–11627. [[CrossRef](#)]
58. Scalmani, G.; Frisch, M.J.; Mennucci, B.; Tomasi, J.; Cammi, R.; Barone, V. Geometries and Properties of Excited States in the Gas Phase and in Solution: Theory and Application of a Time-Dependent Density Functional Theory Polarizable Continuum Model. *J. Chem. Phys.* **2006**, *124*, 094107. [[CrossRef](#)] [[PubMed](#)]
59. Yanai, T.; Tew, D.P.; Handy, N.C. A New Hybrid Exchange–Correlation Functional Using the Coulomb-Attenuating Method (CAM-B3LYP). *Chem. Phys. Lett.* **2004**, *393*, 51–57. [[CrossRef](#)]
60. Figgen, D.; Rauhut, G.; Dolg, M.; Stoll, H. Energy-Consistent Pseudopotentials for Group 11 and 12 Atoms: Adjustment to Multi-Configuration Dirac–Hartree–Fock Data. *Chem. Phys.* **2005**, *311*, 227–244. [[CrossRef](#)]
61. Peterson, K.A.; Puzzarini, C. Systematically Convergent Basis Sets for Transition Metals. II. Pseudopotential-Based Correlation Consistent Basis Sets for the Group 11 (Cu, Ag, Au) and 12 (Zn, Cd, Hg) Elements. *Theor. Chem. Acc.* **2005**, *114*, 283–296. [[CrossRef](#)]
62. Kendall, R.A.; Dunning, T.H.; Harrison, R.J. Electron Affinities of the First-row Atoms Revisited. Systematic Basis Sets and Wave Functions. *J. Chem. Phys.* **1992**, *96*, 6796–6806. [[CrossRef](#)]
63. Caricato, M. Absorption and Emission Spectra of Solvated Molecules with the EOM–CCSD–PCM Method. *J. Chem. Theory Comput.* **2012**, *8*, 4494–4502. [[CrossRef](#)]
64. Chemcraft-Graphical Program for Visualization of Quantum Chemistry Computations. Available online: <https://www.chemcraftprog.com/> (accessed on 18 April 2023).

Disclaimer/Publisher’s Note: The statements, opinions and data contained in all publications are solely those of the individual author(s) and contributor(s) and not of MDPI and/or the editor(s). MDPI and/or the editor(s) disclaim responsibility for any injury to people or property resulting from any ideas, methods, instructions or products referred to in the content.